VISTA Expression on Cancer-Associated Endothelium Selectively Prevents T-cell Extravasation

Luk, S.J.; Schoppmeyer, R.; Ijsselsteijn, M.E.; Somarakis, A.; Acem, I.; Remst, D.F.G.; ... ; Heemskerk, M.H.M.

VISTA Expression on Cancer-Associated Endothelium Selectively Prevents T-cell Extravasation

Sietse J. Luk[1], Rouven Schoppmeyer[2,3,4], Marieke E. Ijsselsteijn[5], Antonios Somarakis[6], Ibtissam Acem[7,8], Dennis F.G. Remst[1], Daan T. Cox[1], Cornelis A.M. van Bergen[1], Inge Briaire-de Bruijn[5], Max L.B. Grönloh[2,4], Werner J. van der Meer[2,4], Lukas J.A.C. Hawinkels[9], Roman I. Koning[10], Erik Bos[10], Judith V.M.G. Bovée[5], Noel F.C.C. de Miranda[5], Karoly Szuhai[10], Jaap D. van Buul[2,3,4], J.H. Frederik Falkenburg[1], and Mirjam H.M. Heemskerk[1]

ABSTRACT

Cancers evade T-cell immunity by several mechanisms such as secretion of anti-inflammatory cytokines, down regulation of antigen presentation machinery, upregulation of immune checkpoint molecules, and exclusion of T cells from tumor tissues. The distribution and function of immune checkpoint molecules on tumor cells and tumor-infiltrating leukocytes is well established, but less is known about their impact on intratumoral endothelial cells. Here, we demonstrated that V-domain Ig suppressor of T-cell activation (VISTA), a PD-L1 homolog, was highly expressed on endothelial cells in synovial sarcoma, subsets of different carcinomas, and immune-privileged tissues. We created an *ex vivo* model of the human vasculature and demonstrated that expression of VISTA on endothelial cells selectively prevented T-cell transmigration over endothelial layers under physiologic flow conditions, whereas it does not affect migration of other immune cell types. Furthermore, endothelial VISTA correlated with reduced infiltration of T cells and poor prognosis in metastatic synovial sarcoma. In endothelial cells, we detected VISTA on the plasma membrane and in recycling endosomes, and its expression was upregulated by cancer cell–secreted factors in a VEGF-A–dependent manner. Our study reveals that endothelial VISTA is upregulated by cancer-secreted factors and that it regulates T-cell accessibility to cancer and healthy tissues. This newly identified mechanism should be considered when using immunotherapeutic approaches aimed at unleashing T cell–mediated cancer immunity.

Introduction

Synovial sarcoma is an aggressive soft-tissue sarcoma that is characterized by a specific driver translocation between chromosomes X and 18, resulting in a fusion of the *SS18* gene with *SSX1*, *SSX2*, or *SSX4* (1). The 10-year cancer-specific survival for patients with metastatic synovial sarcoma is under 10% (2), underscoring the need for effective systemic therapies. Synovial sarcoma responds poorly to immune checkpoint blockade with mAbs against cytotoxic T-lymphocyte associated protein 4 (CTLA-4) and programmed cell death protein 1 (PD-1; refs. 3, 4), which is in line with its low mutational burden (5, 6) that results in a low number of putative neoantigens that can be recognized by autologous T cells. Furthermore, synovial sarcoma is generally poorly infiltrated by T cells (7), whereas its tumor microenvironment is enriched with macrophages displaying immunosuppressive features (8). Removing immunologic barriers that preclude T-cell infiltration into synovial sarcoma could result in an improved clinical outlook for this disease.

In this study, we used imaging mass cytometry (IMC) as a discovery tool to identify mechanisms underlying T-cell exclusion in synovial sarcoma. We demonstrated that in synovial sarcoma and several other cancer types, V-domain Ig suppressor of T-cell activation (VISTA), an immune checkpoint molecule that is homologous to programmed death-ligand 1 (PD-L1) and suppresses T-cell responses *in vitro* and *in vivo* (9–12), is highly expressed on intratumoral endothelial cells (EC). We demonstrate that VISTA acts as an endothelial immune checkpoint molecule that selectively halts T-cell migration across the endothelium.

Materials and Methods

Human materials

All patient materials were collected and used according to the Declaration of Helsinki and Dutch law and regulations. Patient materials were derived from the bone and soft-tissue tumor biobank at Leiden University Medical Center and coded according to the ethical guidelines described in "Code for Proper Secondary Use of Human Tissue in the Netherlands" of the Dutch Federation of Medical Scientific Societies, as reviewed and approved by the Medical Ethical Board Leiden-Den Haag-Delft (B20.034). Written informed consent was acquired from the patients that were included in this biobank. For some patients that were included in the biobank before 2015, a waiver of consent was obtained by the institutional medical ethical board.

[1]Department of Hematology, Leiden University Medical Center, Leiden, The Netherlands. [2]Molecular Cell Biology Lab, Department of Molecular Hematology, Sanquin Research, Amsterdam, the Netherlands. [3]Landsteiner Laboratory, Amsterdam UMC, University of Amsterdam, Amsterdam, the Netherlands. [4]Leeuwenhoek Centre for Advanced Microscopy, Molecular Cytology, Swammerdam Institute for Life Sciences, University of Amsterdam, Amsterdam, the Netherlands. [5]Department of Pathology, Leiden University Medical Center, Leiden, the Netherlands. [6]Department of Radiology, Leiden University Medical Center, Leiden, the Netherlands. [7]Department of Orthopedic Surgery, Leiden University Medical Center, Leiden, the Netherlands. [8]Department of Oncological and Gastrointestinal Surgery, Erasmus MC Cancer Institute, Rotterdam, the Netherlands. [9]Department of Gastroenterology-Hepatology, Leiden University Medical Center, Leiden, the Netherlands. [10]Department of Cell and Chemical Biology, Leiden University Medical Center, Leiden, the Netherlands.

Corresponding Author: Sietse J. Luk, Department of Hematology, Leiden University Medical Center, Leiden, Zuid-Holland 2333 ZA, the Netherlands. E-mail: s.j.luk@lumc.nl; and Mirjam H.M. Heemskerk, E-mail: m.h.m.heemskerk@lumc.nl

Cancer Immunol Res 2023;11:1480–92

doi: 10.1158/2326-6066.CIR-22-0759

Three tissue microarrays (TMA) were created from 71 formalin-fixed paraffin-embedded (FFPE) tumor resections of synovial sarcoma that were derived from 44 patients. Inclusion criteria were all SS18-SSX fusion gene–positive synovial sarcoma samples in our biobank. When possible, three 1.5-mm cores were included from each tumor resection. In cases where limited material was available, 2 or 1 cores were included per tumor, resulting in a total of 201 synovial sarcoma cores. Primary tumors were included that were treatment naïve, as well as primary tumors that were sampled after cytotoxic therapy. Metastatic tumors that did not undergo cytotoxic therapy were included as well. Commercial TMAs with normal and malignant tissues were obtained from Biomax. TMA MNO961 contained the following tissues from healthy individuals (the number in brackets represents the number of samples each from a different patients): adrenal gland [3], urinary bladder [3], bone marrow [1], eye [2], breast [3], cerebellum [3], cerebral cortex [3], 3x fallopian tube [3], esophagus [3], stomach [3], small intestine [3], colon [3], rectum [3], heart [3], kidney [6], liver [3], lung [3], ovary [3], pancreas [3], parathyroid [1], pituitary gland [2], placenta [3], prostate [3], skin [2], spinal cord [2], spleen [2], skeletal muscle [3], testis [3], thymus [3], thyroid [3], tonsil [3], ureter [3], cervix [3] and endometrium [3]. BC000119b contained invasive breast carcinoma [38], lung squamous cell carcinoma [38], colon adenocarcinoma [38], prostate adenocarcinoma [38], and pancreas adenocarcinoma [38]. BC000120a contained stomach adenocarcinoma [38], hepatocellular carcinoma [38], ovary adenocarcinoma [38], endometrioid adenocarcinoma [38], and squamous cell carcinoma of head and neck [38]. BNC17011c contained brain specimens from frontal lobe [3], apical lobe [3], occipital lobe [3], temporal lobe [3], midbrain [3], pons [3], medulla oblongata [3], Thalamus opticus, [3], cerebellum [3], hippocampus [3], callositas [3], optic nerve [3], spinal cord [3], and caudate nucleus [1]. TMA HEN241a contained healthy heart tissues [24].

Imaging mass cytometry

Antibodies were conjugated in-house with Maxpar antibody labeling kits (Fluidigm) according to manufacturer's protocol using 100 μg of antibody per reaction. Antibodies were diluted in 100 μL antibody stabilization buffer (Candor Bioscience, catalog no. 131 050) before use. A full list of antibodies including incubation times and temperatures is summarized in Supplementary Table S1. Formalin-fixed, paraffin-embedded (FFPE) tissue sections were stained for imaging mass cytometry as previously described (13). Shortly, sections were deparaffinized in xylene and rehydrated in a series of ethanol. Heat-mediated antigen retrieval was performed in citrate buffer pH 6.0 (0.1 mol/L sodium citrate; Sigma, catalog no. W302600) in distilled water, adjusted with 0.1 mol/L citric acid (Sigma, catalog no. C0759; to pH 6.0) for 10 minutes using a microwave oven. After cooling, slides were blocked using Superblock PBS Blocking Buffer (Thermo Fisher Scientific, catalog no. 57515), and slides were incubated overnight with anti-CD39. After washing three times in PBS-0.05% Tween (Sigma, catalog no. P1379), a Qdot800-labeled anti-mouse secondary antibody (diluted 1:100, Thermo Fisher Scientific, catalog no. Q-11071MP) was incubated for 1 hour at room temperature, followed by washing and incubation for 5 hours at room temperature with half of the metal-conjugated antibodies. After washing, the second half of the metal-conjugated antibodies was incubated overnight at 4°C, followed by washing. Slides were then incubated with an iridium-labeled DNA intercalator (Fluidigm, catalog no. 201192A), washed with deionized water, and dried before imaging on a Hyperion imaging mass cytometry system (Fluidigm).

Analysis of imaging mass cytometry data

Cell segmentation was performed using Ilastik version 1.3.2 (14) and Cell Profiler version 2.2.0 (15). Pixel classification was performed in Ilastik to create probability maps from the DNA intercalating staining for subsequent segmentation of tumor cells and lymphocytes in Cell Profiler. Combined images with signals from CD31, CD68, and CD204 were used to create probability masks for myeloid and endothelial cells and subsequent segmentation in cell profiler. Masks for both cell types were combined in Cell Profiler. A semiautomated background removal was performed on raw TIFF images for each channel in Ilastik to reduce noise, as was described previously (16), and some markers were excluded because of inadequate staining [Supplementary Table S1 (indicated by *)]. The in-house developed software IMACytE (17) was used to combine imaging data with the cell masks and to calculate mean intensity values for each segmented cell. Single cells were then embedded using hierarchical stochastic neighborhood embedding (hSNE) in Cytosplore version 2.2.1. (18), and density-based clusters were generated that were separated into two groups based on their protein abundance: tumor/stromal cells and immune/endothelial cells. The latter group was further explored by t-distributed SNE (tSNE) in Cytosplore and density-based clustering. IMACytE was used to map identified cell phenotypes back to the original images to investigate tissue distribution of identified phenotypes.

Immunofluorescent labeling of FFPE tissue sections and adherent cells

For immunofluorescent labeling of FFPE tissues, 4-μm-thick FFPE tissue sections were deparaffinized in xylene, rehydrated in a series of ethanol, and heat-mediated antigen retrieval was performed in a Tris-EDTA buffer at pH 9.0 (10 mmol/L TRIS; Sigma, catalog no. T1503), 0.1 mmol/L EDTA [Sigma (catalog no. E5143) in deionized water] in a microwave oven. Slides were blocked using Superblock PBS Blocking Buffer (Thermo Fisher Scientific, catalog no. 57515) for 30 minutes, and primary antibodies were incubated in PBS with 1% BSA (Sigma, catalog no. A7030; PBS-BSA) overnight at 4°C (Supplementary Table S2, "Immunofluorescence in FFPE tissues"). After 3×5-minute washes in PBS, secondary antibodies (Supplementary Table S2, "Secondary antibodies") were incubated for 1 hour at room temperature, followed by 3×5-minute washes in PBS and incubation for 5 minutes with 1 μmol/L 4′,6-diamidino-2-phenylindole (DAPI; catalog no. D9564, Sigma) in PBS. Slides were mounted in prolong gold (Thermo Fisher Scientific, catalog no. P36930). For immunofluorescent labeling of adherent cells, endothelial cells were grown overnight on in-house gelatin-coated glass slides [Start Frost slides, Knittel Glass, coated overnight at 37°C with 0.2% gelatin (BDH Chemicals, Cat. # 44045) in PBS] and then washed two times with cold PBS before fixation with 3.7% formaldehyde (Merck, catalog no. 1.03999.1000) in PBS and permeabilization with either 70% ethanol (1 hour at room temperature) or 0.1% Triton (Sigma, catalog no. T8787) for 10 minutes at room temperature. Slides were washed two times for 2 minutes in PBS-BSA before primary antibody incubation was performed (Supplementary Table S2, "Confocal microscopy") in PBS-BSA for 1 hour at room temperature, followed by 3×5-minute washes and incubation with secondary antibodies Supplementary Table S2, "Secondary antibodies") in PBS-BSA for 30 minutes at room temperature. Slides were washed three times for 5 minutes, incubated for 5 minutes with 1 μmol/L DAPI in PBS, and mounted with Prolong Gold Mounting medium. Slides were scanned using a Zeiss Axio ScanZ1 slide scanner (Zeiss). High-resolution confocal images were acquired using an SP8 scanning confocal microscope (Leica).

Analysis of dual immunofluorescent images

Full-slide scans of TMA slides were loaded into QuPath version 0.2.3 (19) for TMA core annotation and exporting raw fluorescence data as multilayered TIFF files for each individual core. TIFF files were manually inspected for the presence of tissue, morphology, and appropriate CD31 staining as a control for fixation. Samples that did not contain any tissue or showed no CD31 staining were excluded from the analysis. All individual cores were scored by two independent observers as follows: "−" for <5% of vessels positive for VISTA; "+" for 5% to 40% of vessels positive for VISTA; "++" for 40% to 80% of vessels positive for VISTA; and "+++" for >80% of vessels positive for VISTA. The VISTA score per tumor was calculated as the average of all suitable cores, which was rounded to an integer for visualization purposes.

Quantification of T-cell infiltration

CD3-labeled full-slide images were processed into multilayer tiff files per TMA core as described for CD31/VISTA staining in QuPath. In ImageJ (20), tumor regions were manually annotated. Composite images of CD3 and the adjacent empty channel were transferred to the pixel classification tool of Ilastik version 1.3.2. (14) and trained for CD3 signal. Generated probability maps and annotated tumor maps were used to quantify intratumoral T-cell numbers per mm^2 of tumor in Cell Profiler (15).

Analysis of single-cell mRNA sequencing data

Mapped read counts per cell from 12 human synovial sarcoma samples were downloaded from the Gene Expression Omnibus (GSM3770931; ref. 21) and analyzed using the Seurat V3 pipeline in R-studio (22). tSNE embeddings were generated to visualize the expression of lineage markers and the gene coding for VISTA, *VSIR*. Phenotypes of single cells were adopted from the original publication of Jerby-Arnon and colleagues and shown with color scale on the single-cell tSNE embedding (21).

Cell culture

Human umbilical cord endothelial cells (HUVEC) were isolated from umbilical cords according to Jaffe and colleagues (23) and kindly provided by A. van Oeveren-Rietdijk and H.C. de Boer (Department of Nephrology, Leiden University Medical Center, Leiden, the Netherlands). HUVECs and EC-RF24 endothelial cells (24) were cultured in gelatin-coated dishes (cell culture dishes coated for at least 30 minutes at 37°C with 0.2% gelatin in PBS) in M199 medium (Gibco, catalog no. 31150030) supplemented with 20% FBS (Sigma F7524), bovine pituitary extract (50 μg/mL, Gibco, catalog no. 13028014), heparin (10 IU/mL, LEO), and 1% penicillin/streptomycin (P/S; Lonza, catalog no. 17–602E). Primary HUVECs were used up to passage 5. SYO-1 synovial sarcoma cells were cultured in Iscove's modified Dulbecco medium (IMDM; Lonza 12–722F) supplemented with 10% FBS and 1% P/S. SYO-1 cells were a kind gift from Akira Kawai, National Cancer Center Hospital (Tokyo, Japan; ref. 25). SYO-1–conditioned HUVEC medium was generated by plating 2×10^6 SYO-1 cells in a T75 flask and growing to overconfluency for 5 days, while replacing the medium daily. At day 5, medium was replaced by 20 mL HUVEC medium, and SYO-1 cells were cultured for an additional 72 hours, after which the supernatant was harvested and stored at −80°C.

Peripheral blood mononuclear cell isolation

Peripheral blood mononuclear cells (PBMC) were obtained from fresh blood provided by a total of 10 healthy anonymous donors at Sanquin Blood Supply. Blood was diluted 1:2 with isolation buffer (PBS + 2 mmol/L EDTA) and up to 35 mL was layered over 15 mL of Ficoll Paque Plus (Sigma, catalog no. GE17–1440–02), followed by centrifugation at 400 × *g* for 40 minutes at room temperature with the brake off. PBMCs in the interphase were harvested and transferred into a fresh tube that was filled (up to 50 mL) using isolation buffer. After three centrifugation steps [(i) 350 × *g* for 10 minutes; (ii) 200 × *g* for 10 minutes; (iii) 200 × *g* for 10 minutes], cells were counted and used for magnetic bead isolation as described below.

Monocyte isolation

Monocytes were isolated from PBMCs derived from fresh human heparinized blood provided by three voluntary anonymous donors (Sanquin Blood Supply) using Negative Selection with Magnetic Beads (Miltenyi Biotec, catalog no. 130–096–537) and LS columns (catalog no. 130–042–401, Miltenyi Biotec) according to the manufacturer's instructions using PBS supplemented with 2 mmol/L EDTA and 0.5% FCS as running buffer. After isolation, cells were resuspended to 1×10^6 cells/mL in PBS supplemented with 2 mmol/L EDTA and 0.5% FCS and were kept on ice. Immediately before injection into the flow-based *in vitro* assays, 1×10^6 cells were centrifuged and resuspended in 1 mL of HEPES flow buffer/medium [20 mmol/L HEPES (132 mmol/L NaCl, 6 mmol/L KCL, 1 mmol/L $CaCl_2$, 1 mmol/L $MgSO_4$, 1.2 mmol/L K_2HPO_4, 1 g/L D-glucose (all from Sigma Aldrich), and 0.5% (w/v) human serum albumin (Sanquin)] and thoroughly resuspended to avoid clumping.

Neutrophil isolation

Neutrophils were isolated from fresh human heparinized blood provided by three voluntary anonymous donors (Sanquin Blood Supply) using Percoll (Merck, catalog no. P1644) density centrifugation. PBMCs were diluted (1:1) with 5% (v/v) TNC (trisodium citrate) in PBS. The diluted whole blood was pipetted carefully onto 12.5 mL of Percoll (at room temperature, density = 1.076 g/mL). Tubes were centrifuged at 450 × *g* without brake for 20 minutes. The fraction containing RBCs and polymorphonuclear cells (PMN) was further processed by erythrocyte lysis using cold isotonic lysis buffer (155 mmol/L NH_4Cl, 10 mmol/L $KHCO_3$, 0.1 mmol/L EDTA at pH 7.4) in distilled water on ice. This step was repeated once. After centrifugation at 450 × *g* for 10 minutes at 4°C, PMNs were washed once with PBS and centrifuged again at 450 × *g* for 5 minutes at 4°C before resuspension in HEPES medium. Neutrophils were kept at room temperature and were used for experiments for no longer than 4 hours before injection into the flow-based *in vitro* assays, warmed at 37°C for 10 minutes in an Eppendorf tube in a water bath.

T-cell isolation and recovery

$CD8^+$ and $CD4^+$ T cells were isolated from fresh PBMCs from six donors using the negative $CD8^+$ or $CD4^+$ T-cell Isolation Kit (catalog no. 130–096–495/130–096–533, Miltenyi Biotec) and LS columns (catalog no. 130–042–401, Miltenyi Biotec) according to the manufacturer's instructions using the same buffer as for monocyte isolation. Isolated T cells were counted and placed in an incubator overnight in RPMI1640 (Thermo Fisher Scientific, catalog no. 61870036) medium with 10% FCS and 1% P/S at a density of 2×10^6 cells/mL.

Cloning and retroviral transduction

Total RNA was isolated using the Micro RNaqueous Kit (Ambion) before DNA was fragmented with DNAse (Ambion) and removed by RNeasy Mini Kit (Qiagen). cDNA synthesis was performed using oligo dT primers with M-MLV reverse transcriptase (Invitrogen). A retroviral vector for overexpression of *VISTA* was created by amplifying

full-length *VISTA* cDNA from isolated $CD14^+$ cells with primers containing ECOR1 restriction sites for cloning into a MP71 eGPF-expressing vector (26). eGFP-tagged VISTA constructs were created by amplifying *VISTA* and eGFP separately and performing fusion PCR. eGFP was attached with a GGGGGS linker to the C-terminus of full-length *VISTA*. eGFP-tagged-VISTA constructs were cloned into an MP71-markerless vector (26). Primers and details of the PCR reactions are described in Supplementary Table S3. XL-2 Blue ultracompetent cells (Agilent, catalog no. 200150) were used for clonal selection and amplification of vectors. Vectors were checked by bidirectional Sanger sequencing to ensure correct cloning and insertion of the target sequences into vector backbones. After purification with the PureYield Plasmid Miniprep system (Promega, catalog no. A1222), retroviral vectors were transfected into Phoenix-GALV cells (27) using FuGene HD Transfection Reagent (Promega, E2311). Virus-containing supernatant was collected 48 hours after transfection. For retroviral transduction, non–tissue culture–treated plates (Greiner, catalog no. 657 185 or 662 102) were coated overnight with 30 μg/mL retronectin (TaKaRa Bio, catalog no. T100B) and blocked for 30 minutes with 1% human serum albumin (Albuman, Sanquin Plasma Products BV). The harvested virus was centrifuged at 2,000 × *g* for 20 minutes at 4°C, supernatant was removed, and endothelial cells were added at 70% confluency in their appropriate culture medium and cultured overnight before trypsinization (Gibco, catalog no. 25300). After five days of culture, cells were enriched for the retroviral vector containing eGFP using a BD FACSAria III 4 L cell sorter (BD Biosciences). Cell purity was >95% for cells used in experiments as described below.

Stimulation of endothelial cells and qPCR

HUVECs were plated in 12-well dishes (0.1–0.2 × 10^6 cells/well) and grown to confluency in 3 to 4 days, while replacing medium every 48 hours. Stimulation was performed by adding 2 mL SYO-1 conditioned-medium, or 2 mL medium that was supplemented with VEGF-A 165 (50–100 ng/mL, Sigma, catalog no. V5765–10 μg) or placental growth factor (100 ng/mL, BioLegend, catalog no. 765202). To the abovementioned stimulation conditions, bevacizumab (10 μg/mL, Pfizer) or SU5416 (1 μmol/L, WuXi AppTec) were added or not added. During stimulation, medium was refreshed every 48 hours, except for SYO-1 conditioned medium, which was refreshed every 24 hours. Cells were harvested after the indicated time intervals for RNA isolation using the ReliaPrep RNA Miniprep System (Promega, catalog no. Z6012). cDNA was synthesized from 1,000 ng mRNA using oligo DT primers with M-MLV reverse transcriptase (Invitrogen, catalog no. 28025–013). qPCR was performed on a Roche LightCycler 480 using the FastStart Taq DNA Polymerase Kit from Sigma-Aldrich (catalog no. 12032945001) and EvaGreen from Biotium (catalog no. 310000). Primer sequences and conditions are described in Supplementary Table S4. Target gene expression was measured in triplicate, and expression was normalized against the average of three housekeeping genes (*GUSB*, *VSP29*, and *PSMB4*) using the ΔC_t method.

Flow cytometry

For flow cytometry and intracellular staining of VISTA, HUVECs were resuspended using trypsin and fixed using 1% paraformaldehyde (PFA, Apotheek AZL) before permeabilization for 30 minutes with perm buffer [0.2% saponin and 0.1% HSA (Sanquin) in PBS]. Primary VISTA antibody (Cell Signaling Technology, #64953) was incubated for 30 minutes at room temperature in perm buffer, followed by two washing steps perm buffer and incubation with secondary goat anti-rabbit Alexa Fluor 647 antibody (Invitrogen, catalog no. A21244, diluted 1:1,600 in perm buffer) for 30 minutes at room temperature, followed by two washes of 5 minutes in perm buffer. Cells were resuspended in perm buffer and acquired on a Fortessa cytometer (BD Biosciences).

Electron microscopy

Primary HUVECs transduced with VISTA-eGFP were fixed in PIPES, HEPES, EGTA, and magnesium sulphate heptahydrate (PHEM) buffer (28) containing 2% formaldehyde (EMS, catalog no. 157–8) and 0.2% glutaraldehyde (EM grade, EMS catalog no. 16019) for 2 hours. The fixed samples were embedded in 12% gelatin (type A, bloom 300, Sigma) and cut with a razor blade into cubes (0.5 mm^3). The sample blocks were immersed in phosphate buffer containing 2.3 mol/L sucrose for 3 hours. The sample blocks were then mounted on aluminum pins and submerged and stored in liquid nitrogen. For ultrathin sectioning, frozen samples were mounted in a cryo-ultramicrotome (Leica) at 158 K. Samples were trimmed to yield squared blocks with a front face of about 200 × 200 μm. Using a diamond knife (Diatome) and antistatic device (Leica), a ribbon of 60-nm-thick sections was produced that was retrieved from the cryo-chamber with a droplet of 1.15 mol/L sucrose containing 1% methylcellulose. After thawing, the sections were transferred to a specimen grid previously coated with formvar/carbon (Agar Scientific, catalog no. AGS162). The sections attached to the grid were left for 30 minutes on the surface of 2% gelatin in phosphate buffer at 37°C, after which they were rinsed on droplets of PBS at room temperature. The sections were then labeled with the primary anti-eGFP (Supplementary Table S2, "Electron microscopy"), rinsed with PBS, followed by labeling with 10-nm protein A–coated gold particles (CMC, Utrecht University, Utrecht, the Netherlands; catalog no. PAG10nm/S). Subsequently, the labeled sections on the grid were embedded in 2% methylcellulose and 0.4% uranyl acetate (pH 4.5) and air-dried. Electron microscopy images were recorded using a Tecnai 12 TEM (FEI company) equipped with an EAGLE 4×4K digital camera using a magnification of 13,000×.

Flow-based *in vitro* transmigration assay

HUVECs were stimulated overnight with TNFα (PeproTech, catalog no. 300–01A, 10 ng/mL) in EGM-2 (PromoCell, catalog no. C-22011) containing endothelial cell growth supplement (Promocell, catalog no. C-39216) and 1% P/S (Thermo Fisher Scientific, catalog no. 15140122). In experiments using the VISTA blocking antibody onvatilimab (MedChem Express, catalog no. HY-P99040), the endothelial cells were incubated prior to flow-based experiments with the antibody at a concentration of 100 μg/mL for 60 minutes at 37°C. TNFα-/antibody-treated HUVECs were then subjected to flow with HEPES buffer [20 mmol/L HEPES, 132 mmol/L NaCl, 6 mmol/L KCL, 1 mmol/L $CaCl_2$, 1 mmol/L $MgSO_4$, 1.2 mmol/L K_2HPO_4, 1 g/L D-glucose, and 0.5% (w/v) human serum albumin]. HEPES flow buffer was prepared fresh for every experiment, filtered, warmed to 37°C, and used on the same day. A flow rate of 0.5 mL/minute, corresponding to approximately 0.8 dyne/cm^2, was set on a table-top pump (Prosense) with a 60 mL syringe with Luer-Lock tip (BD Biosciences). Endothelial cells were exposed to the flow rate indicated for 10 minutes prior to the injection of 1-mL leukocytes (isolated monocytes, neutrophils, and $CD8^+$ T cells) with a concentration of 1 × 10^6 cells per mL in RPMI containing 10% FBS and 1% P/S. Imaging of live cells was performed using a Zeiss Axiovert 200 Widefield microscope with a HXP lighting unit and incubation (37°C and 5% CO_2). For each channel, multiple random positions were recorded and analyzed as discussed below.

Flow-based transmigration assay analysis

Recorded image series were analyzed using Fiji is just ImageJ version 2.11.0 (20). For transmigration efficiency, all adherent T cells were counted, as well as all transmigration events. Transendothelial migration efficiency was calculated as the percentage of adherent cells that transmigrated. For distant transendothelial migration, all transmigrating T cells in a series were counted and marked, and the number of transmigrated T cells that performed diapedesis at a location that required crossing of at least two different endothelial junctions were categorized as distantly transmigrating. For this assessment, individual transmigrated T cells were traced back manually to their point of adhesion, and the crossed junctions were counted. Distantly transmigrating T cells were reported as a percentage of all transmigrated T cells within an image series. For each experimental flow assay condition, between 5 and 10 image series were recorded in parallel from the same flow channel. All series recorded were analyzed.

Statistics, data visualization, and survival analysis

Data were plotted using Graphpad Prism 9.0.1 (LCC). For statistical testing in transendothelial migration assays, unpaired *t* tests were performed. For testing differences in T-cell infiltration between different VISTA-scored cores, a Mann–Whitney *U* test was performed. A χ^2 Test was used to compare proportions of high endothelial VISTA between primary and metastatic disease. The Kaplan–Meier estimator from SPSS version 25 (IBM) was used to estimate the survival for patients with primary and metastatic synovial sarcoma stratified by endothelial VISTA expression. Overall survival was defined as the time interval between resection and date of death, taking censoring into account. Differences in survival were evaluated with the log-rank test if proportional hazard assumption was met, or the Peto–Wilcoxon test if the proportional hazard assumption was violated. The proportional hazard assumption was assessed visually. $P \leq 0.05$ was considered statistically significant.

Data availability

The expression data that were analyzed in this study are available from Gene Expression Omnibus (GEO) under GSM3770931 (21). The data generated in this study are available upon request from the corresponding author.

Results

VISTA is highly expressed on the endothelium of synovial sarcoma

To study the immune cell composition and prevalence of immune checkpoint molecules in synovial sarcoma, imaging mass cytometry (IMC) with a 39-antibody panel was applied on nine tumor resections from 8 patients with synovial sarcoma (**Fig. 1A**; Supplementary Table S1). A total of 25 regions of interest were analyzed. Cell segmentation, as described in the Materials and Methods section, resulted in a total of 286,314 segmented cells that were visualized using hSNE (Supplementary Fig. S1). The segmented cells were separated into 244,579 single tumor/stromal cells and 41,735 single immune cells/endothelial cells based on major lineage markers (Supplementary Fig. S1). tSNE was used to investigate the immune cells and endothelial cells in detail (**Fig. 1B**; Supplementary Fig. S2). The most prevalent immune checkpoint molecule expressed in synovial sarcoma was VISTA, which was present on endothelial cells of 9/9 tumors to a varying degree (**Fig. 1B** and **C**). VISTA was expressed to a lesser extent on lymphocytes and myeloid cells, whereas plasma cells that were present in two tertiary lymphoid structures, defined as an area of dense colocalization of B cells and T cells, of two cases showed strong expression of VISTA (**Fig. 1B**). None of the 9 tumors showed expression of VISTA on tumor cells (**Fig. 1B** and **C**; Supplementary Fig. S1). For other immune checkpoints that were included, only PD-1 was expressed, and its expression was restricted to a subset of T cells present in the two tertiary lymphoid structures scanned (Supplementary Figs. S2 and S3). We detected no expression of IDO, ICOS, or PD-L1.

To confirm our findings at the mRNA level, we used publicly available, single-cell RNA sequencing data (21) generated from 12 synovial sarcomas from 9 patients to investigate the association between *VISTA* expression and specific cell types. Mapped read counts per cell were downloaded, converted to counts per million (CPM), and tSNE plots of single cells were created on the basis of total gene expression. Mapping the expression of *VISTA* revealed its expression in endothelial cells of all synovial sarcoma cases, as well as in myeloid cells and, to a lesser extent, in lymphocytes, confirming the high expression of this immune checkpoint in the endothelium of synovial sarcoma (**Fig. 2**).

VISTA is highly expressed on the endothelium of immune-privileged tissues and a subset of human cancers

To quantify the expression of VISTA on endothelial cells of healthy tissues and multiple cancer types including synovial sarcoma, we evaluated coimmunofluorescent detection of CD31 and VISTA on 103 normal tissue samples and 402 cancer samples of various histologic subtypes. In synovial sarcoma, 47 of 66 (71%) tumors demonstrated substantial expression of VISTA on the endothelium, with more than 40% of the microvessels scored positive for VISTA (VISTA++ or VISTA+++; **Fig. 3A–D**). In 3 of 44 patients with synovial sarcoma, VISTA expression was detected on tumor cells (Supplementary Fig. S4). These three cases had biphasic synovial sarcoma, composed of epithelial and spindle-cell compartments, and VISTA was only expressed in the epithelial component of the tumor. Confocal scanning microscopy revealed VISTA expression to be located at the membrane and exhibited a granular expression pattern in the cytoplasm in both endothelial cells and tumor cells (**Fig. 3E**; Supplementary Fig. S4). In other tumor types, endothelial VISTA was most abundant in lung squamous cell carcinoma, invasive breast carcinoma, and stomach adenocarcinoma, with endothelial VISTA scoring of ++ or +++ in 18%, 12%, and 11% of cases, respectively. In normal tissues, VISTA was most prominently expressed on the endothelial cells of immune-privileged tissues, such as the brain (100% ++/+++), cardiac muscle (86% ++/+++), and the female reproductive system (ovary, fallopian tube, cervix, endometrium, and healthy breast; 57% ++/+++), whereas VISTA expression was absent in other tissues such as skin and lung (**Fig. 3A** and **F–K**). Although the placenta highly expressed VISTA, it was located on the syncytiotrophoblasts, CD31-negative cells lining the fetal–maternal border, but not on endothelial cells (**Fig. 3I**). These data demonstrate that VISTA is highly expressed on endothelial cells within a subset of cancers, most frequently in synovial sarcoma, but also on immune-privileged tissues, thereby supporting its role in suppressing immunity.

VISTA is located on the plasma membrane of endothelial cells and stored in recycling endosomes

To investigate in which intracellular compartment VISTA is localized in endothelial cells, we applied immunofluorescent labeling with

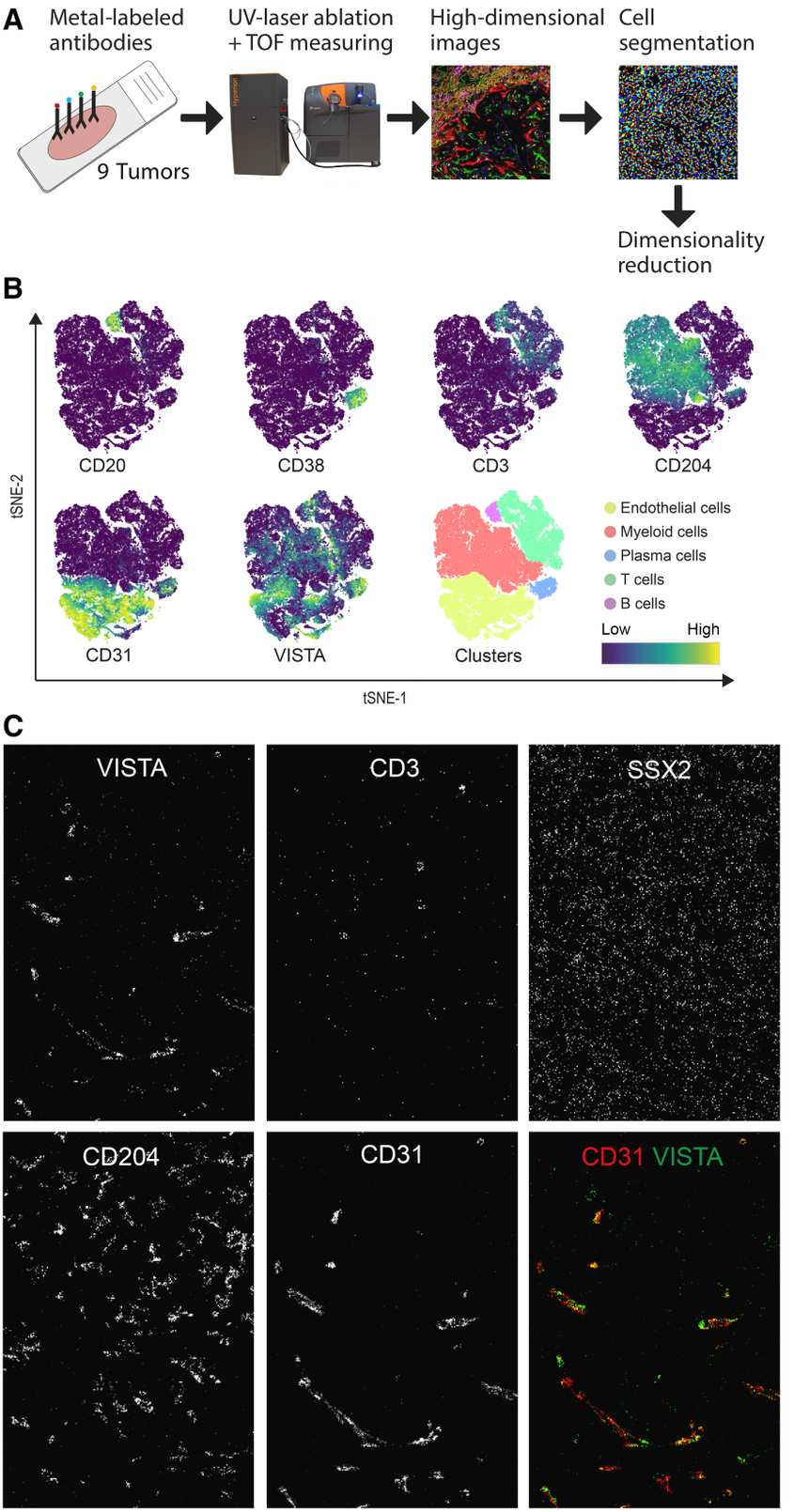

Figure 1.

Imaging mass cytometry reveals VISTA expression on endothelial cells in synovial sarcoma. Combined imaging mass cytometry data from 25 regions from 9 synovial sarcomas of 8 patients. **A,** Experimental workflow. **B,** tSNE plots of immune cells and endothelial cells. Antibody staining intensity per cell is shown for CD20, CD38, CD3, CD204, CD31, and VISTA with color scale. Major lineages were identified by the shown lineage markers and cells were clustered as shown in the bottom right panel. **C,** Imaging mass cytometry images showing staining of VISTA, CD3, SSX2 (tumor marker), CD204, and CD31 in the same tumor area. Bottom right, composite of CD31 and VISTA.

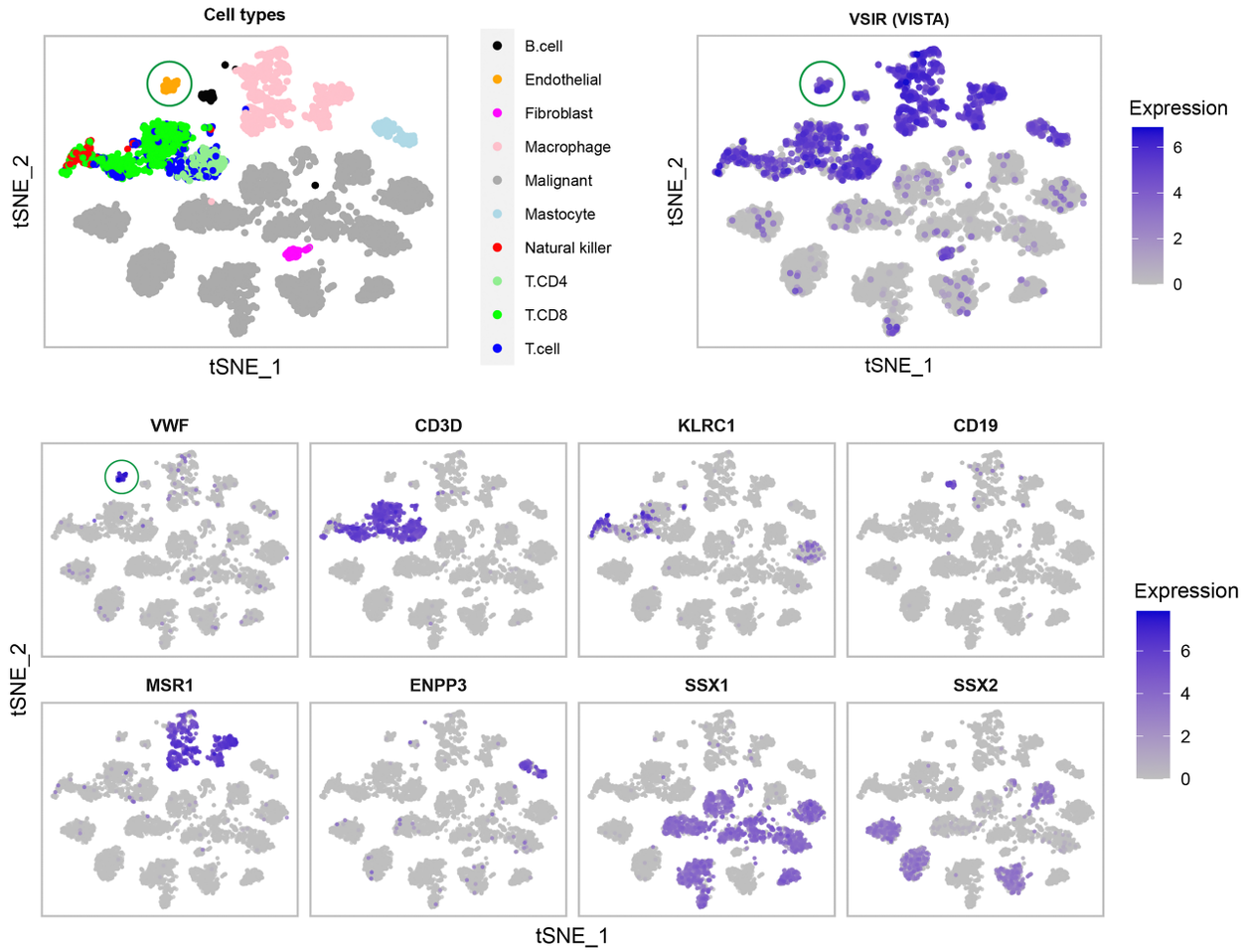

Figure 2.

VISTA is expressed at the mRNA level in endothelial cells in synovial sarcoma. Publicly available single-cell RNA sequencing data from 12 synovial sarcomas derived from 9 patients were plotted as tSNE maps based on gene expression levels of all genes. Cell phenotypes as identified by Jerby-Arnon and colleagues (21) are shown in the top left by color coding of the tSNE. Expression of *VISTA* is shown in the top right by color scale. Small panels show the expression of lineage marker genes by color scale. Endothelial cells are shown in orange (top left) and are marked with a green circle (first three panels).

cell compartment–specific markers on *VISTA*-transduced HUVECs. We observed an almost complete overlap between VISTA and transferrin receptor (TfR) expression, indicating that VISTA was located within recycling endosomes and on the plasma membrane (**Fig. 4A**). VISTA did not colocalize with Weibel–Palade bodies, early endosomes, lysosomes, or $CD63^+$ vesicles (Supplementary Fig. S5). In placental syncytiotrophoblasts, VISTA was also colocalized with TfR (**Fig. 4A**), demonstrating that the colocalization was not an artifact of retroviral transduction. To confirm the localization of VISTA at the plasma membrane and recycling endosomes, we transduced HUVECs with a vector encoding the VISTA protein with an eGFP tag and performed immunogold labeling of eGFP, followed by electron microscopy. This revealed localization of the tagged VISTA protein at the plasma membrane and in vesicles that were concentrated in the Golgi area but were also captured during fusion with the plasma membrane (**Fig. 4B** and **C**). These data indicate exchange of VISTA between these compartments and is in accordance with localization in recycling endosomes. Thus, in endothelial cells, VISTA is expressed on the plasma membrane and in recycling endosomes.

Synovial sarcoma cells upregulate VISTA in endothelial cells in a VEGF-A–dependent manner

On the basis of the specific upregulation of VISTA in endothelial cells of synovial sarcoma, we investigated whether synovial sarcoma tumor cells induced VISTA expression in endothelial cells. Wild-type HUVECs were incubated with cell culture supernatants from synovial sarcoma cells. After 6 days of incubation, *VISTA* expression was upregulated 5-fold in HUVECs (**Fig. 4D**). This effect was blocked by addition of the VEGF-A neutralizing antibody bevacizumab and the VEGF-receptor 2 tyrosine kinase inhibitor SU5416 (**Fig. 4D**), indicating that the effect was VEGF-A/VEGFR2-dependent. Although short-term stimulation with VEGF-A (up to 24 hours) did not result in upregulation of *VISTA*, prolonged stimulation resulted in up to 20-fold upregulation of *VISTA* in primary HUVECs, suggesting long-time VEGF signaling is needed for VISTA upregulation (**Figs. 4D**; Supplementary Fig. S6A). To investigate whether increased mRNA expression of *VISTA* translated into elevated VISTA protein expression, we performed flow cytometry on unstimulated and VEGF-A–stimulated HUVECs. Five-day VEGF-A–stimulated HUVECs showed increased

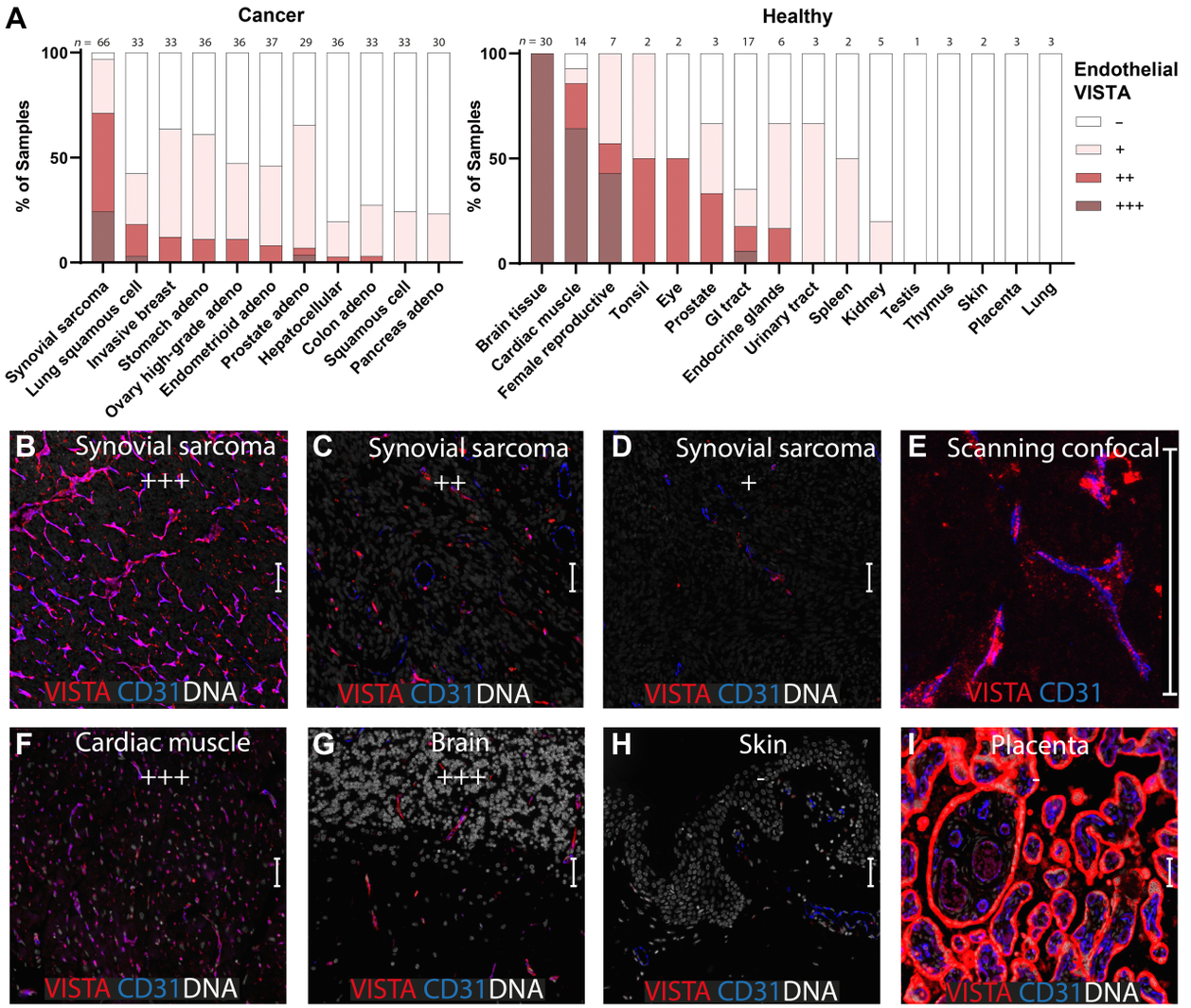

Figure 3.

The immune checkpoint VISTA is highly expressed on the endothelial cells of immune-privileged tissues and a subset of human cancer. **A,** The amount of VISTA-positive blood vessels as percentage of total blood vessels was scored in both cancer and healthy tissues. Left, endothelial VISTA in synovial sarcoma and several carcinomas. Right, endothelial VISTA in healthy tissues. –, <5% VISTA-positive vessels; + 5%–40% VISTA-positive vessels; ++, 40%–80% VISTA-positive vessels; +++, >80% VISTA-positive vessels. Numbers on top of bars represent number of biological samples scored per tissue type. Female reproductive organs: ovary, fallopian tube, cervix, endometrium and healthy breast. Adeno, adenocarcinoma. **B–D,** Representative wide-field fluorescent images of VISTA (red) and CD31 (blue) in FFPE synovial sarcoma sections scoring +++ (**B**), ++ (**C**), and + (**D**) DAPI is shown in white. **E,** Maximum projection of scanning confocal microscopy images show a granular staining pattern of VISTA in endothelial cells (**D**). **F–I,** Same as **B** and **C** but in healthy tissue sections of cardiac muscle (**F**), brain (**G**), skin (**H**), and placenta (**I**). Note that expression of VISTA in the placenta is located in the syncytiotrophoblasts, cells lining the fetal–maternal interface but not endothelial cells as scored in **A**. Scale bars, 50 μm.

VISTA protein expression compared with unstimulated HUVECs (Supplementary Fig. S6B and S6C). Summarizing, synovial sarcoma cells upregulated *VISTA* expression in endothelial cells in a VEGF-A–dependent manner via a paracrine mechanism.

Endothelial VISTA abrogates transendothelial migration of T cells

On the basis of the prominent expression of VISTA on endothelial cells in immune-privileged tissues and synovial sarcoma, we hypothesized that VISTA inhibits T-cell migration over endothelial layers, thereby preventing extravasation and migration of T cells into surrounding tissues and cancer. To investigate whether VISTA could inhibit transendothelial migration, we created an *in vitro* model of the human vasculature and performed transendothelial migration assays under physiologic flow conditions (**Fig. 5A**). We used endothelial layers composed of primary HUVECs either transduced with VISTA and GFP or with GFP only (MOCK control; **Fig. 5B**; Supplementary Movies S1 and S2). Freshly isolated $CD8^+$ T cells from 6 healthy individuals were introduced to HUVEC monolayers in a pump-based flow chamber providing unidirectional laminar flow and sheer forces resembling those in capillaries. No difference was found in $CD8^+$ T-cell adherence to MOCK- or VISTA-transduced HUVECs (**Fig. 5C**).

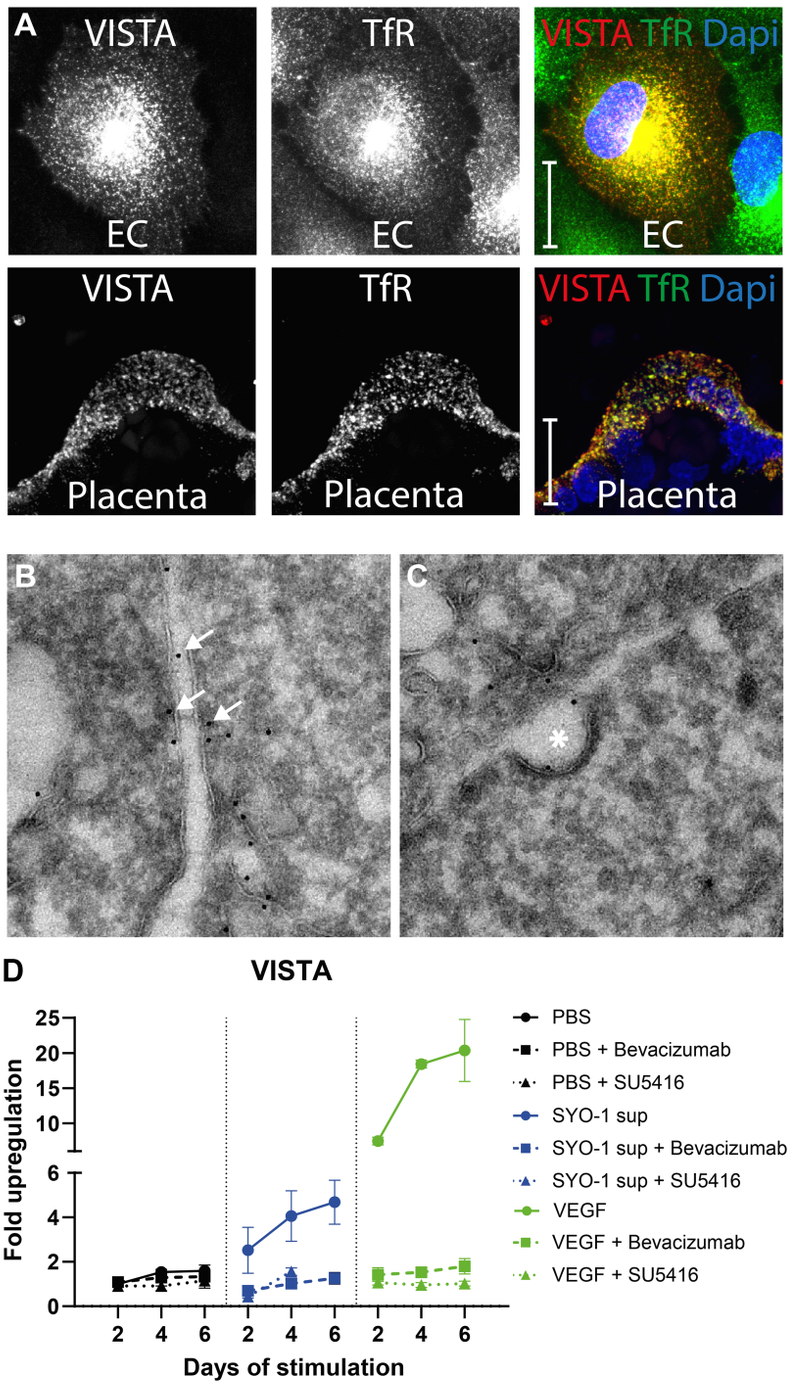

Figure 4.

In endothelial cells, VISTA is stored in recycling endosomes and upregulated by tumor-secreted VEGF-A. **A,** Maximum projection of confocal imaging stacks of fluorescently labeled VISTA (left) and transferrin receptor (middle) in a VISTA-transduced endothelial cell and a FFPE placenta tissue. Right, composite images. Scale bar, 20 µm. **B** and **C,** Electron microscopy images of HUVECs transduced with nanogold-labeled eGFP-tagged VISTA protein. **B,** Gold nanoparticles labeling the introduced VISTA protein at the plasma membrane are illustrated with white arrows. **C,** An invagination or fusion at the level of the plasma membrane, showing the presence of nanogold-labeled VISTA is marked by an asterisk. **D,** Confluent monolayers of HUVECs were stimulated with HUVEC medium that was supplemented with PBS (black), synovial sarcoma conditioned medium (blue), or with VEGF-A (50 ng/mL, green). Stimulation was performed without blocking (circles) or combined with the VEGF-A blocking antibody bevacizumab (10 µg/mL) (rectangles) or the VEGF-Receptor 2 kinase inhibitor SU5416 (1 µmol/L; triangles). Expression of *VISTA* was analyzed using RT-qPCR at different time points. *VISTA* expression is shown as fold change to PBS at the first time point as calculated with the ΔC_t method with three housekeeping genes (HKG) as control. Prolonged stimulation with SYO-1 supernatant combined with SU5416 was toxic to HUVECs resulting in not enough live cells to isolate RNA for this condition after 6 days. Data are presented as combined data from two experiments using HUVECs from different donors. Error bars, range of measurements for each condition. Prolonged stimulation with a combination of synovial sarcoma conditioned medium and SU5416 was toxic for HUVECs which is why we were unable to measure VISTA expression after 6 days for this condition.

Upon attachment, T cells can either stay rounded and static, or they can polarize to migrate laterally over the endothelial layer (**Fig. 5B**). A significant decrease in T-cell polarization was observed in T cells attaching to VISTA-expressing endothelium compared with MOCK control ($P < 0.001$; **Fig. 5D**), indicating less activation of the adhering T cells in the presence of VISTA. Expression of VISTA on endothelial cells significantly reduced the transendothelial migration of adhering T cells from 57% to 9% when HUVECs expressed VISTA ($P < 0.001$; **Fig. 5E**). In addition, distant diapedesis, defined as an event in which a T cell crosses two or more endothelial cell–cell junctions before transmigrating, was observed in 41% of all transmigration events through VISTA-transduced endothelium compared with 5% in the control condition ($P < 0.001$, **Fig. 5F**), indicating an inadequate level of protransmigration signaling between adhering T cells and endothelial cells. To investigate whether the inhibition of T-cell migration by VISTA was caused by a direct interaction of VISTA with a receptor on T cells, we repeated the transendothelial migration assays with the VISTA

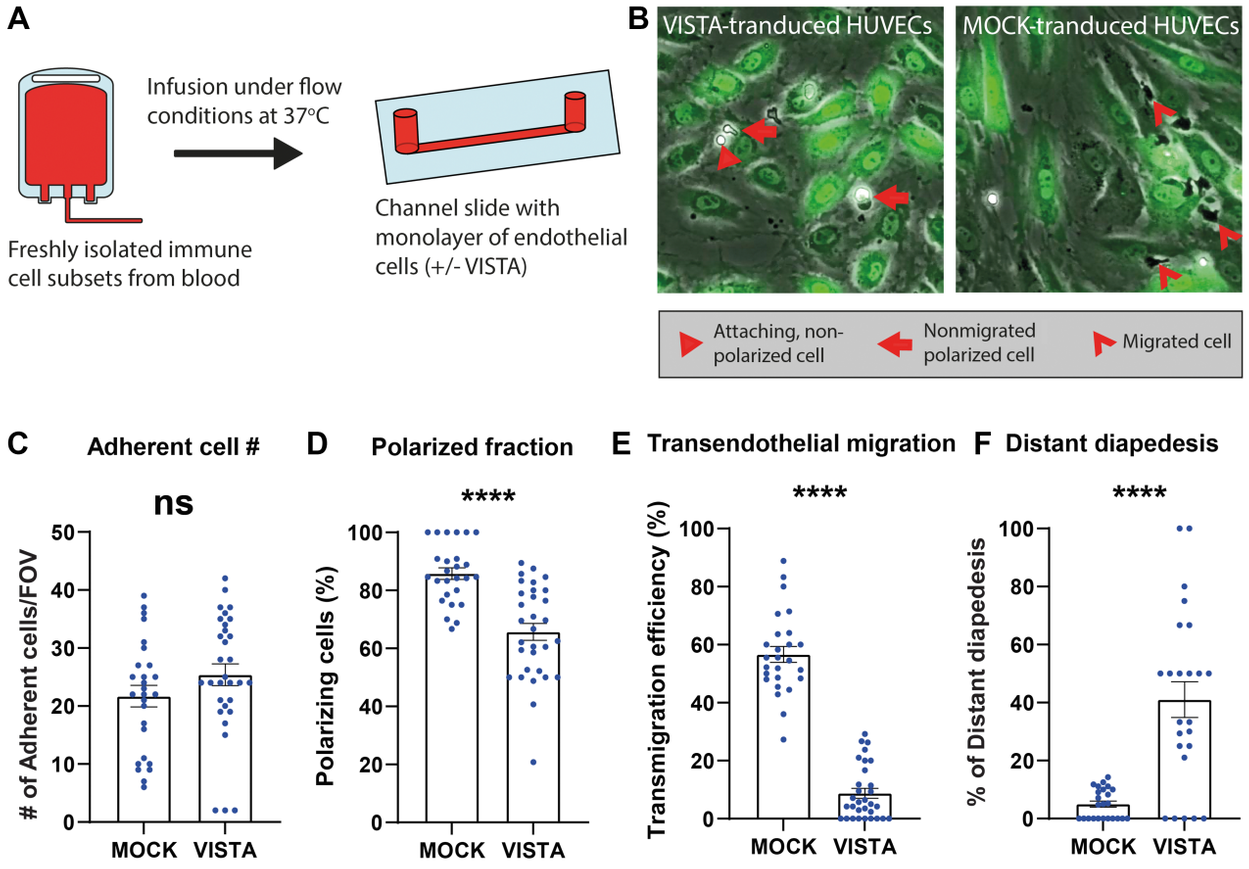

Figure 5.

Expression of VISTA on endothelial cells strongly reduces transendothelial migration of T cells without affecting adhesion. **A,** Schematic overview of experimental workflow. **B,** Captures from real-time imaging of transendothelial migration of CD8 T cells over a monolayer of VISTA (left) or mock (right) transduced endothelial cells. **C–F,** Results of flow-based transendothelial migration assay using HUVECs that were transduced with a full-length VISTA construct (VISTA) or a mock construct (MOCK) and isolated CD8 T cells. Each datapoint represents a field of view (FOV) in which an area of the artificial blood vessel was imaged for the duration of 20 minutes. Data are combined from 6 unrelated CD8 T-cell donors. **C,** Number of adherent cells per field of view. **D,** Percentage of adhering T cells that show polarization and lateral migration upon endothelial cell contact. **E,** Percentage of adhering cells that transmigrated through the endothelial monolayer. **F,** Percentage of all transmigration events that happened after the transmigrated T cell crossed more than two endothelial cell–cell junctions. Error bars, SEM. ****, $P < 0.001$; ns, not statistically significant.

antagonistic antibody onvatilimab. Preincubation of MOCK-transduced HUVECs with onvatilimab did not affect transendothelial migration. However, it was able to restore transendothelial migration of $CD8^+$ T cells over VISTA-expressing endothelium, thus showing the effect was caused by a direct interaction of VISTA with T cells (Supplementary Fig. S7).

In addition to blocking $CD8^+$ T-cell transendothelial migration, VISTA also blocked transendothelial migration of $CD4^+$ T cells (Supplementary Fig. S8A and S8B). To assess whether VISTA on endothelial cells specifically blocked the migration of T cells or blocked migration of other leukocyte subsets, we introduced freshly isolated monocytes and neutrophils from three donors in the transendothelial migration assay under the same conditions. Similar to T cells, the expression of VISTA on endothelial cells did not alter the attachment of monocytes or neutrophils to endothelial cells. However, in contrast to our observations for the T cells, no effect on the number of monocytes and neutrophils crossing VISTA-expressing endothelial cells was measured (Supplementary Fig. S8C and S8F). Combined, these data demonstrate that VISTA expressed on endothelial cells locally downregulates T-cell polarization upon endothelial cell contact and selectively prevents transendothelial T-cell migration.

Endothelial VISTA correlates with T-cell infiltration in synovial sarcoma and poor survival in metastatic disease

To investigate whether VISTA's inhibition of T-cell infiltration observed *in vitro* correlated to decreased T-cell infiltration in patients with synovial sarcoma, we performed immunofluorescence for CD3 in consecutive sections of our synovial sarcoma TMAs and quantified the number of intratumoral T cells/mm^2 of tumor tissue (see Materials and Methods section for details). The number of T cells/mm^2 of tumor tissues was significantly lower in cores with ++ or +++ endothelial VISTA compared with cores with low − or + endothelial VISTA ($P = 0.0026$; **Fig. 6A**), suggesting that endothelial VISTA impaired T-cell infiltration *in vivo*. To investigate whether endothelial VISTA influenced clinical outcomes in patients with synovial sarcoma, we compared overall survival of synovial sarcoma tumors with high VISTA scoring (at least one of three cores +++) and tumors that had lower endothelial VISTA. Within our cohort of patients with primary synovial sarcoma ($n = 33$), there was no significant correlation

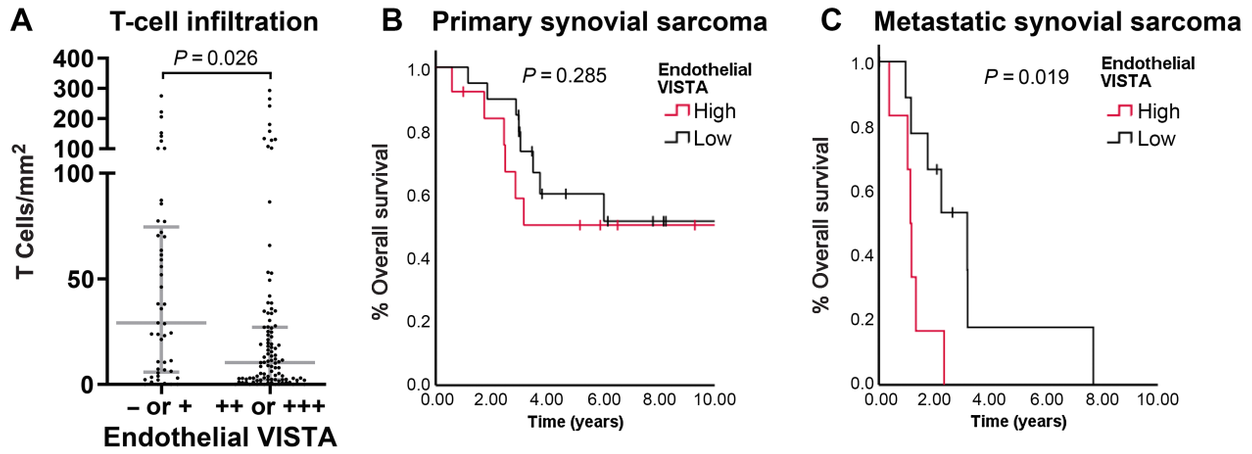

Figure 6.

Endothelial VISTA correlates with reduced T-cell infiltration and poor survival in metastatic synovial sarcoma. **A,** Correlation of T-cell counts per mm^2 of tumor tissue and VISTA scoring per synovial sarcoma TMA core. Error bars, median and interquartile range. **B** and **C,** Association between high (at least one core +++) endothelial VISTA expression and survival in patients with primary synovial sarcoma (**B**) and patients with metastatic synovial sarcoma (**C**). High endothelial VISTA significantly correlated with poor survival in metastatic synovial sarcoma but not in primary synovial sarcoma.

between high endothelial VISTA and overall survival ($P = 0.285$; **Fig. 6B**). Although there was no difference in high VISTA scoring between primary and metastatic tumors (13/33 and 6/16, respectively, $P = 0.898$), high endothelial VISTA correlated significantly with decreased survival in metastatic synovial sarcoma ($n = 16$ patients; $P = 0.019$; **Fig. 6C**). Together, these data suggest a different role for endothelial VISTA in metastatic and primary disease and highlight the clinical relevance of endothelial VISTA in patients with synovial sarcoma.

Discussion

In this study, we identified the PD-L1 homolog VISTA as a highly expressed immune checkpoint molecule on endothelial cells of synovial sarcoma and subsets of other cancer types. We showed that paracrine secretion of VEGF-A, which was secreted by synovial sarcoma, as well as other tumors, upregulated VISTA in endothelial cells and was located on the plasma membrane and in recycling endosomes. Importantly, VISTA correlated with reduced T-cell infiltration and selectively prevented transendothelial migration of T cells *in vitro*, highlighting its role in the exclusion of T cells from immune-privileged tissues and cancer.

The expression of VISTA on intratumoral endothelial cells was previously detected in pancreatic cancer, ovarian cancer, cervical cancer, and gastric cancer by IHC (29–33). We added a quantitative comparison of endothelial VISTA between different subtypes of human cancer and found that synovial sarcoma exhibited high expression of endothelial VISTA compared with other cancers. Furthermore, we found that endothelial VISTA was expressed in healthy immune-privileged tissues, particularly the brain and cardiac muscle, which is in line with earlier data that describes endothelial VISTA in brain tissues (34). The distribution of endothelial VISTA suggests a role in immune exclusion, which was further supported by the high expression of VISTA on syncytiotrophoblasts in placenta, the fetal cells that are in direct contact with the maternal blood flow and form a physical barrier against migration of immune cells.

Endothelial VISTA correlated with poor survival in metastatic synovial sarcoma but not in primary disease. This unexpected finding could be explained by the different determinants of survival between these two patient groups: in primary disease, survival is mainly determined by surgical margins and intrinsic potential of the specific synovial sarcoma to metastasize, whereas in metastatic disease, surgery is often performed with a palliative intent and other undetected metastases are often present at other locations in the body. The effect of local and systemic immunity on tumor progression may be more profound in the latter situation, which could explain the bigger impact of endothelial VISTA on survival in metastatic disease. Due to the limited sample size, we were unable to account for surgical margins in our analysis.

Although VISTA interacts with other cells at the plasma membrane, a large proportion of VISTA was stored in the recycling endosomes of endothelial cells. This suggests that VISTA is constantly stored and kept "at a ready-state" for shuttling to the site of cell–cell contact when an immune cell interacts with a VISTA-expressing endothelial cell. Interestingly, in mouse macrophages, VISTA is also stored within recycling endosomes, suggesting a similar mechanism of cell surface regulation by myeloid cells and endothelial cells (35). Future studies using fluorescently tagged VISTA in live-cell imaging may shed further light on the role of recycling endosomes and VISTA signaling by endothelial cells and myeloid cells.

Multiple *in vitro* studies have demonstrated that VISTA inhibits T-cell functions, and an ongoing discussion is taking place on whether VISTA inhibits T cells as a ligand that binds to a receptor on T cells or whether it functions as a signaling receptor on T cells themselves (9–11, 36). Evidence has been shown for both, and multiple proteins have been shown to bind VISTA, including VSIG3/IgSF11 (37, 38), and PSGL-1 (39). In this study, we provide evidence that during synapse formation in diapedesis, VISTA interacts with an unidentified receptor on T cells which results in less T-cell polarization and transendothelial migration.

We demonstrated that synovial sarcoma cells upregulated VISTA on endothelial cells in a VEGF-A–dependent manner. Because the majority of synovial sarcoma overexpress VEGF-A, this could explain the high expression of VISTA we found in the endothelium of this tumor (40, 41). The fact that transendothelial migration of T cells, but not of neutrophils and monocytes, was inhibited by VISTA, suggests

that VISTA selectively excludes T cells from immune-privileged tissues and cancer, thereby shaping the immune composition. This is in line with the composition of infiltrating immune cells in synovial sarcoma, which is characterized by limited numbers of T cells and large numbers of tumor-associated macrophages, which are partly derived from peripheral blood monocytes (8, 42). Further evidence that VISTA is involved in regulating T-cell infiltration comes from two previous studies. In a mouse model of multiple sclerosis, VISTA knockout results in severe deterioration of disease and increased T-cell infiltration in the brain (43). Another study shows increased infiltration of T cells into the mouse B16 melanoma model after administration of VISTA blocking antibodies (44).

In this study, we linked VEGF-A to expression of VISTA on endothelial cells and T-cell infiltration, which suggests that existing anti-VEGF therapies and immune checkpoint blockade could work synergistically. Indeed, in the mouse CT26 colorectal cancer model, targeting both VEGF and PD-L1 results in increased infiltration of $CD8^+$ T cells and better tumor control, whereas either treatment alone had no effect (45). A clinical trial is currently evaluating the addition of the VEGF-A blocking antibody bevacizumab to PD-L1 inhibition and chemotherapy in biliary tract cancer (46).

Although mAb therapies blocking VISTA are primarily developed to target immunosuppressive tumor-associated macrophages and T cells, our study demonstrates an additional mechanism of action for blocking VISTA. Targeting VISTA with mAbs in cancer may lead to enhanced T-cell infiltration, which could induce potent antitumor responses. Treatment of solid cancer with genetically modified T cells is currently hampered by limited infiltration of modified T cells into tumors. In cancers with VISTA on endothelial cells, combining anti-VISTA treatment with adoptive cell therapies is likely to improve adoptively transferred T cells to infiltrate into solid tumors, thereby overcoming one of the main hurdles these therapies currently face. However, our data also raises potential safety issues. Because VISTA is expressed on endothelial cells of the heart and the brain, targeting VISTA might result in T-cell infiltration into these tissues. Although no dose-related toxicities were observed in preclinical models (47), our observations should be considered in clinical studies, as blocking VISTA with mAbs may lead to unacceptable toxicities in heart and brain (NCT04475523, NCT05082610, NCT02671955).

Collectively, our data demonstrate that VISTA is expressed on the intratumoral endothelial cells of synovial sarcoma and healthy immune-privileged tissues, where it selectively excludes T cells from transmigration, thereby shaping the immune landscape toward a more tolerogenic microenvironment.

Authors' Disclosures

L.J. Hawinkels reports grants from Tracon Pharmaceuticals outside the submitted work. J.V. Bovee reports grants from Tracon Pharmaceuticals outside the submitted work. No disclosures were reported by the other authors.

Authors' Contributions

S.J. Luk: Conceptualization, data curation, formal analysis, funding acquisition, investigation, visualization, methodology, writing–original draft, project administration. **R. Schoppmeyer:** Formal analysis, investigation, methodology. **M.E. Ijsselsteijn:** Resources, investigation, methodology. **A. Somarakis:** Resources, software, formal analysis, methodology. **I. Acem:** Data curation, formal analysis, validation, methodology. **D.F.G. Remst:** Validation, investigation. **D.T. Cox:** Investigation. **C.A.M. van Bergen:** Data curation, investigation, visualization, methodology. **I. Briaire de Bruijn:** Methodology. **M.L.B. Grönloh:** Formal analysis, Investigation. **W.J. van der Meer:** Formal analysis, investigation. **L.J.A.C. Hawinkels:** Resources, methodology. **R.I. Koning:** Methodology. **E. Bos:** Investigation, methodology. **J.V.M.G. Bovee:** Writing–review and editing. **N.F.C.C. de Miranda:** Supervision, writing–review and editing. **K. Szuhai:** Methodology, writing–review and editing. **J.D. van Buul:** Supervision, methodology. **J.H.F. Falkenburg:** Supervision, writing–review and editing. **M.H.M. Heemskerk:** Supervision, funding acquisition, writing–review and editing.

Acknowledgments

We thank Marjolijn Hameetman for her support with the imaging mass cytometry. We thank Hetty de Boer and Annemarie van Oeveren-Rietdijk for providing HUVECs. We thank Ruud Wijdeven for providing antibodies against TfR, CD63, and EEA1. Eveline Jonge-Muller helped with the culture of primary HUVECs. We are grateful to Annelies van der Laan, Lennard Voortman, and Karien Wiesmeijer from the LUMC Light and Electron Microscopy Facility for helping with immunofluorescence microscopy. We thank Akira Kawai for providing the SYO-1 cell line. We thank Anne Wouters for testing the onvatilimab antibody in T-cell assays prior to its use in transendothelial migration assays. This work was supported by Leiden University Medical Centre MD/PHD trajectory grant (to S.J. Luk and M.H.M. Heemskerk)

The publication costs of this article were defrayed in part by the payment of publication fees. Therefore, and solely to indicate this fact, this article is hereby marked "advertisement" in accordance with 18 USC section 1734.

Note

Supplementary data for this article are available at Cancer Immunology Research Online (http://cancerimmunolres.aacrjournals.org/).

Received September 23, 2022; revised April 14, 2023; accepted September 1, 2023; published first September 11, 2023.

References

1. WHO/IARC. WHO Classification of tumours editorial board, soft tissue and bone tumours. Fifth edition. Lyon, France: IARC; 2020.
2. Sultan I, Rodriguez-Galindo C, Saab R, Yasir S, Casanova M, Ferrari A. Comparing children and adults with synovial sarcoma in the surveillance, epidemiology, and end results program, 1983 to 2005: an analysis of 1268 patients. Cancer 2009;115:3537–47.
3. Maki RG, Jungbluth AA, Gnjatic S, Schwartz GK, D'Adamo DR, Keohan ML, et al. A pilot study of anti-CTLA4 antibody ipilimumab in patients with synovial sarcoma. Sarcoma 2013;2013:168145.
4. Tawbi HA, Burgess M, Bolejack V, Van Tine BA, Schuetze SM, Hu J, et al. Pembrolizumab in advanced soft-tissue sarcoma and bone sarcoma (SARC028): a multicentre, two-cohort, single-arm, open-label, phase 2 trial. Lancet Oncol 2017;18:1493–501.
5. He M, Abro B, Kaushal M, Chen L, Chen T, Gondim M, et al. Tumor mutation burden and checkpoint immunotherapy markers in primary and metastatic synovial sarcoma. Hum Pathol 2020;100:15–23.
6. van Oost S, Meijer DM, Kuijjer ML, Bovee J, de Miranda N. Linking immunity with genomics in sarcomas: is genomic complexity an immunogenic trigger? Biomedicines 2021;9:1048.
7. Luk SJ, van der Steen DM, Hagedoorn RS, Jordanova ES, Schilham MW, Bovee JV, et al. PRAME and HLA Class I expression patterns make synovial sarcoma a suitable target for PRAME specific T-cell receptor gene therapy. Oncoimmunology 2018;7:e1507600.
8. Oike N, Kawashima H, Ogose A, Hotta T, Hatano H, Ariizumi T, et al. Prognostic impact of the tumor immune microenvironment in synovial sarcoma. Cancer Sci 2018;109:3043–54.
9. Wang L, Rubinstein R, Lines JL, Wasiuk A, Ahonen C, Guo Y, et al. VISTA, a novel mouse Ig superfamily ligand that negatively regulates T cell responses. J Exp Med 2011;208:577–92.
10. Lines JL, Pantazi E, Mak J, Sempere LF, Wang L, O'Connell S, et al. VISTA is an immune checkpoint molecule for human T cells. Cancer Res 2014;74:1924–32.

11. Mulati K, Hamanishi J, Matsumura N, Chamoto K, Mise N, Abiko K, et al. VISTA expressed in tumour cells regulates T cell function. Br J Cancer 2019;120: 115–27.
12. Flies DB, Han X, Higuchi T, Zheng L, Sun J, Ye JJ, et al. Coinhibitory receptor PD-1H preferentially suppresses CD4(+) T cell-mediated immunity. J Clin Invest 2014;124:1966–75.
13. Ijsselsteijn ME, van der Breggen R, Farina Sarasqueta A, Koning F, de Miranda N. A 40-marker panel for high dimensional characterization of cancer immune microenvironments by imaging mass cytometry. Front Immunol 2019;10:2534.
14. Berg S, Kutra D, Kroeger T, Straehle CN, Kausler BX, Haubold C, et al. ilastik: interactive machine learning for (bio)image analysis. Nat Methods 2019;16: 1226–32.
15. Kamentsky L, Jones TR, Fraser A, Bray MA, Logan DJ, Madden KL, et al. Improved structure, function and compatibility for CellProfiler: modular high-throughput image analysis software. Bioinformatics 2011;27:1179–80.
16. Ijsselsteijn ME, Somarakis A, Lelieveldt BPF, Hollt T, de Miranda N. Semi-automated background removal limits data loss and normalizes imaging mass cytometry data. Cytometry A 2021;99:1187–97.
17. Somarakis A, Van Unen V, Koning F, Lelieveldt B, Hollt T. ImaCytE: visual exploration of cellular micro-environments for imaging mass cytometry data. IEEE Trans Vis Comput Graph 2021;27:98–110.
18. van Unen V, Hollt T, Pezzotti N, Li N, Reinders MJT, Eisemann E, et al. Visual analysis of mass cytometry data by hierarchical stochastic neighbour embedding reveals rare cell types. Nat Commun 2017;8:1740.
19. Bankhead P, Loughrey MB, Fernandez JA, Dombrowski Y, McArt DG, Dunne PD, et al. QuPath: open source software for digital pathology image analysis. Sci Rep 2017;7:16878.
20. Schindelin J, Arganda-Carreras I, Frise E, Kaynig V, Longair M, Pietzsch T, et al. Fiji: an open-source platform for biological-image analysis. Nat Methods 2012;9: 676–82.
21. Jerby-Arnon L, Neftel C, Shore ME, Weisman HR, Mathewson ND, McBride MJ, et al. Opposing immune and genetic mechanisms shape oncogenic programs in synovial sarcoma. Nat Med 2021;27:289–300.
22. Stuart T, Butler A, Hoffman P, Hafemeister C, Papalexi E, Mauck WM III, et al. Comprehensive integration of single-cell data. Cell 2019;177:1888–902.
23. Jaffe EA, Nachman RL, Becker CG, Minick CR. Culture of human endothelial cells derived from umbilical veins. Identification by morphologic and immunologic criteria. J Clin Invest 1973;52:2745–56.
24. Fontijn R, Hop C, Brinkman HJ, Slater R, Westerveld A, van Mourik JA, et al. Maintenance of vascular endothelial cell-specific properties after immortalization with an amphotrophic replication-deficient retrovirus containing human papilloma virus 16 E6/E7 DNA. Exp Cell Res 1995;216:199–207.
25. Kawai A, Naito N, Yoshida A, Morimoto Y, Ouchida M, Shimizu K, et al. Establishment and characterization of a biphasic synovial sarcoma cell line, SYO-1. Cancer Lett 2004;204:105–13.
26. Schambach A, Wodrich H, Hildinger M, Bohne J, Krausslich HG, Baum C. Context dependence of different modules for posttranscriptional enhancement of gene expression from retroviral vectors. Mol Ther 2000;2:435–45.
27. Overbaugh J, Miller AD, Eiden MV. Receptors and entry cofactors for retroviruses include single and multiple transmembrane-spanning proteins as well as newly described glycophosphatidylinositol-anchored and secreted proteins. Microbiol Mol Biol Rev 2001;65:371–89.
28. Schliwa M, van Blerkom J. Structural interaction of cytoskeletal components. J Cell Biol 1981;90:222–35.
29. Hou Z, Pan Y, Fei Q, Lin Y, Zhou Y, Liu Y, et al. Prognostic significance and therapeutic potential of the immune checkpoint VISTA in pancreatic cancer. J Cancer Res Clin Oncol 2021;147:517–31.
30. Liao H, Zhu H, Liu S, Wang H. Expression of V-domain immunoglobulin suppressor of T cell activation is associated with the advanced stage and presence of lymph node metastasis in ovarian cancer. Oncol Lett 2018;16:3465–72.
31. Kuang L, He Y. Potential value of V-domain Ig suppressor of T-cell activation for assessing progn osis in cervical cancer and as a target for therapy. Int J Clin Exp Pathol 2020;13:26–37.
32. Boger C, Behrens HM, Kruger S, Rocken C. The novel negative checkpoint regulator VISTA is expressed in gastric carcinoma and associated with PD-L1/PD-1: a future perspective for a combined gastric cancer therapy? Oncoimmunology 2017;6:e1293215.
33. Zong L, Zhou Y, Zhang M, Chen J, Xiang Y. VISTA expression is associated with a favorable prognosis in patients with high-grade serous ovarian cancer. Cancer Immunol Immunother 2020;69:33–42.
34. Borggrewe M, Grit C, Den Dunnen WFA, Burm SM, Bajramovic JJ, Noelle RJ, et al. VISTA expression by microglia decreases during inflammation and is differentially regulated in CNS diseases. Glia 2018;66:2645–58.
35. ElTanbouly MA, Croteau W, Noelle RJ, Lines JL. VISTA: a novel immunotherapy target for normalizing innate and adaptive immunity. Semin Immunol 2019; 42:101308.
36. ElTanbouly MA, Zhao Y, Nowak E, Li J, Schaafsma E, Le Mercier I, et al. VISTA is a checkpoint regulator for naive T cell quiescence and peripheral tolerance. Science 2020;367:eaay0524.
37. Wang J, Wu G, Manick B, Hernandez V, Renelt M, Erickson C, et al. VSIG-3 as a ligand of VISTA inhibits human T-cell function. Immunology 2019;156:74–85.
38. Yang W, Padkjaer SB, Wang J, Sun Z, Shan B, Yang L, et al. Construction of a versatile expression library for all human single-pass transmembrane proteins for receptor pairings by high throughput screening. J Biotechnol 2017;260:18–30.
39. Johnston RJ, Su LJ, Pinckney J, Critton D, Boyer E, Krishnakumar A, et al. VISTA is an acidic pH-selective ligand for PSGL-1. Nature 2019;574:565–70.
40. Feng Q, Guo P, Wang J, Zhang X, Yang HC, Feng JG. High expression of SDF-1 and VEGF is associated with poor prognosis in patients with synovial sarcomas. Exp Ther Med 2018;15:2597–603.
41. Wakamatsu T, Naka N, Sasagawa S, Tanaka T, Takenaka S, Araki N, et al. Deflection of vascular endothelial growth factor action by SS18-SSX and composite vascular endothelial growth factor- and chemokine (C-X-C motif) receptor 4-targeted therapy in synovial sarcoma. Cancer Sci 2014;105:1124–34.
42. Zhou J, Tang Z, Gao S, Li C, Feng Y, Zhou X. Tumor-associated macrophages: recent insights and therapies. Front Oncol 2020;10:188.
43. Wang L, Le Mercier I, Putra J, Chen W, Liu J, Schenk AD, et al. Disruption of the immune-checkpoint VISTA gene imparts a proinflammatory phenotype with predisposition to the development of autoimmunity. Proc Natl Acad Sci USA 2014;111:14846–51.
44. Le Mercier I, Chen W, Lines JL, Day M, Li J, Sergent P, et al. VISTA regulates the development of protective antitumor immunity. Cancer Res 2014;74:1933–44.
45. Xue L, Gao X, Zhang H, Tang J, Wang Q, Li F, et al. Antiangiogenic antibody BD0801 combined with immune checkpoint inhibitors achieves synergistic antitumor activity and affects the tumor microenvironment. BMC Cancer 2021;21:1134.
46. Hack SP, Verret W, Mulla S, Liu B, Wang Y, Macarulla T, et al. IMbrave 151: a randomized phase II trial of atezolizumab combined with bevacizumab and chemotherapy in patients with advanced biliary tract cancer. Ther Adv Med Oncol 2021;13:17588359211036544.
47. Thakkar D, Paliwal S, Dharmadhikari B, Guan S, Liu L, Kar S, et al. Rationally targeted anti-VISTA antibody that blockades the C-C' loop region can reverse VISTA immune suppression and remodel the immune microenvironment to potently inhibit tumor growth in an Fc independent manner. J Immunother Cancer 2022;10:e003382.